

# Phase separation kinetics in compressible polymer solutions: Computer simulation of the early stages

Peter Virnau<sup>1</sup>, Marcus Müller<sup>1</sup>, Luis González MacDowell<sup>2</sup>,  
and Kurt Binder<sup>1</sup>

<sup>1</sup>Institut für Physik, Johannes Gutenberg–Universität Mainz,  
Staudinger Weg 7, 55099 Mainz, Germany

<sup>2</sup>Dpto. de Química Física, Facultad de Cc. Químicas,  
Universidad Complutense, 28040 Madrid, Spain

October 25, 2018

## Abstract

A coarse-grained model for solutions of polymers in supercritical fluids is introduced and applied to the system of hexadecane and carbon dioxide as a representative example. Fitting parameters of the model to the gas-liquid critical point properties of the pure systems, and allowing for a suitably chosen parameter that describes the deviation from the Lorentz-Berthelot mixing rule, we model the liquid-gas and fluid-fluid unmixing transitions of this system over a wide range of temperatures and pressures in reasonable agreement with experiment. Interfaces between the polymer-rich phase and the gas can be studied both at temperatures above and below the end point of the triple line where liquid and vapor carbon dioxide and the polymer rich phase coexist. In the first case interfacial adsorption of fluid carbon dioxide can be demonstrated. Our model can also be used to simulate quenches from the one-phase to the two-phase region. A short animation and a series of snapshots help to visualize the early stages of bubble nucleation and spinodal decomposition. Furthermore we discuss deviations from classical nucleation theory for small nuclei.

PACS: 64.60.Qb, 82.20.Wt, 05.70.Fh, 61.41.+e

# 1 Introduction

The phase behavior of polymer-solvent systems has important application in the industry for the production and processing of many kinds of plastic materials [1, 2, 3, 4, 5, 6]. An example is the formation of solid polystyrene foams [3, 4, 5, 6]. In addition, both the understanding of the equilibrium phase diagram of these systems and the kinetic mechanism of phase separation are challenging problems of statistical mechanics. On the one hand, variation of the molecular weight of the polymer (i.e. the “chain length” of the flexible linear macromolecule,  $N$ ) offers a control parameter that leaves intermolecular forces invariant, and hence allows a more stringent test of the theory than would be possible for small molecule systems. On the other hand, it is crucial to take the compressibility of the system fully into account, since for practical reasons one normally wishes to use supercritical fluids (e.g.,  $\text{CO}_2$ ) as a solvent [1, 2, 3, 4, 5, 6]. Then small changes of the pressure result in a large variation of the solvent density, and this fact obviously facilitates applications. While for an incompressible polymer solution (as it is modelled, for instance, by the well-known Flory-Huggins lattice theory [7, 8, 9, 10]) the early stages of phase separation can only be studied if one realizes a rapid temperature quench from a state in the one phase region into the miscibility gap (cf. Fig. 1a), for compressible polymer solutions it is possible to induce phase separation by an (experimentally much more convenient) pressure jump (cf. Fig. 1b). Of course, in Fig. 1 we have made the tacit assumption that including the pressure does not change the qualitative form of the phase diagram, i.e., the point  $(T_c, x_c)$  in  $(T, x, p)$ -space becomes a line  $(T_c(p), x_c(p))$  or, expressed in the appropriate inverse functions,  $(p_c(T), x_c(T))$ , respectively (Fig. 1b). In reality, the situation is more complicated, since one must treat both the densities of  $\text{CO}_2$  and hexadecane as two coupled order parameters, which both play a crucial role in the possible phase transitions (remember that for the pure solvent at its critical point gas-liquid phase separation starts). As a result, it can happen that both gas-liquid and liquid-liquid phase separation are present in the phase diagram, leading to the occurrence of a triple line (Fig. 2) [11]. As will be discussed below, the presence of the triple line has a profound influence on the interface properties and hence the nucleation behavior in the system.

The present paper is devoted to a study of the early stages of phase separation kinetics in such systems by computer simulation. We use a coarse-grained model for mixtures of hexadecane and carbondioxide as an archetypical example. The reason for the choice of this particular system is the fact that recently extensive experiments on nucleation in this system have been performed [12]. In Sec. 2, we shall briefly describe the model and the simulation techniques. Sec. 3 presents the relevant static equilibrium properties, in particular, the phase diagram and the properties of planar interfaces separating coexisting phases. Sec. 4 describes simulations of quenching experiments under different conditions, that lead either to nucleation and growth or spinodal decomposition. Sec. 5 summarizes our conclusions.

## 2 Model and Simulation Techniques

A fully atomistic simulation of mixtures of hexadecane ( $C_{16}H_{34}$ ) and carbon-dioxide ( $CO_2$ ), which aims at both establishing phase diagrams as a function of the three variables  $T, p$  and  $x$ , and the study of phase transition kinetics under various conditions, would be an extremely formidable problem. The potentials for the length of the covalent bonds in these molecules (as well as the potentials for bond angles) are very stiff. Hence, an extremely short time step (of the order of about 1 fs) would be required in a Molecular Dynamics (MD) simulation. In a corresponding Monte Carlo (MC) simulation only very small random displacements of atoms would be admissible. Thus, for liquid alkanes it is a quite common and well-established practice to integrate  $CH_2$ -groups (as well as the  $CH_3$  end groups) into “united atoms” [13], and also to work with a fixed C-C bond length. These simplifications already reduce the necessary computer time by a factor of 100. However, we have estimated that even for such a simplified model computer resources as they are available today still are not yet sufficient. Thus it was chosen to simplify the model even further, representing  $CO_2$  by a single pseudo-atom, and representing  $C_{16}H_{34}$  by a flexible chain of 5 subsequent effective segments, each of which then contains roughly 3 successive C-C bonds. All such effective monomeric units interact with a truncated and shifted Lennard Jones (LJ) potential,

$$V_{LJ}(r) = 4\epsilon_{hh}[(\frac{\sigma_{hh}}{r})^{12} - (\frac{\sigma_{hh}}{r})^6 + \frac{127}{16384}], \quad r \leq r_c = 2 \cdot 2^{1/6}\sigma, \quad (1)$$

while  $V_{LJ}(r > r_c) = 0$ . Subsequent effective monomers along a chain are in addition exposed to a finitely extensible nonlinear elastic (FENE) potential [14]

$$V_{FENE}(r) = -33.75\epsilon_{hh} \ln[1 - (\frac{r}{1.5\sigma_{hh}})^2] \quad (2)$$

The constants in this potential are chosen such that the most favorable distance between bonded neighbors is  $0.96 \sigma_{hh}$ , while the preferred distance between non-bonded effective monomers is  $2^{1/6} \sigma_{hh} \approx 1.12 \sigma_{hh}$ . This mismatch is desirable to prevent crystallization at high densities [15], which is appropriate for glass-forming polymers [3, 4, 5, 6].

The parameters  $\sigma_{hh}$ ,  $\epsilon_{hh}$  set the scales for energy and length of our hexadecane model. Since we wish that our model fits the thermodynamic properties of this material in the fluid phase as faithfully as possible, we have adjusted them such that the critical temperature  $T_c = 723$  K and the critical density  $\rho_c = 0.21$  g/cm<sup>3</sup> of hexadecane are correctly reproduced. In simulations, a critical point can be computed by a finite size scaling study of the liquid-gas transition along the lines of the techniques proposed by Wilding et al. [16]. A comparison of critical temperature and density in Lennard-Jones units with the experimental values yields  $\epsilon_{hh} = 5.787 \cdot 10^{-21}$  J,  $\sigma_{hh} = 4.523 \cdot 10^{-10}$  m [17, 18].

Since the description of hexadecane is thus already reduced to a crudely coarse-grained model, it would not make sense to keep all atomistic detail for

carbon dioxide. Thus the CO<sub>2</sub> molecule is also coarse-grained into a point particle, and we require an interaction potential between CO<sub>2</sub> molecules of exactly the same LJ form as in Eq. (1), but with parameters  $\varepsilon_{cc}$ ,  $\sigma_{cc}$ . Requiring once more that the critical temperature and density of real CO<sub>2</sub> are correctly reproduced we obtained [17]  $\varepsilon_{cc} = 4.201 \cdot 10^{-21}$  J, and  $\sigma_{cc} = 3.693 \cdot 10^{-10}$  m. It is clear that this procedure ignores some physical effects, e.g., the fact that the CO<sub>2</sub> molecules carry electrical multipole moments is completely neglected. Nevertheless our model not only describes the gas-liquid coexistence curve of hexadecane and CO<sub>2</sub> over a reasonable temperature range [17], but also other data (like the critical pressure, or the temperature dependence of the surface tension near  $T_c$  [18]).

Of course, the choice of interaction parameters between CO<sub>2</sub> and hexadecane is more subtle. We model the interaction between the pseudoatoms representing CO<sub>2</sub> and the pseudoatoms representing three subsequent CH<sub>2</sub> groups again by a LJ potential of the form Eq. (1), but now with parameters  $\varepsilon_{hc}$ ,  $\sigma_{hc}$ . It then remains to find an optimal choice for these parameters. The simplest choice would be the well-known Lorentz-Berthelot mixing rule [19]

$$\varepsilon_{hc} = \sqrt{\varepsilon_{hh} \varepsilon_{cc}}, \quad \sigma_{hc} = (\sigma_{hh} + \sigma_{cc})/2 \quad . \quad (3)$$

However, when one tries the choice Eq. (3) the resulting phase diagram of our model system would be of type I in the classification scheme of Van Konynenburg and Scott [20, 21] (i.e., the critical points of pure hexadecane and CO<sub>2</sub> are connected by a critical line of the mixture system. Liquid-liquid phase separation does not exist and thus there is no three phase coexistence). However, experimentally it is known [22] that alkane – CO<sub>2</sub> mixtures exhibit a type I – phase behavior only for very short alkanes, while for hexadecane – CO<sub>2</sub> mixtures the phase diagram is of type III. Instead of a connecting line we rather observe a topology as shown in Fig. 3 [17, 23]. In the (p,T) projection of the phase diagram, a critical line emerges from the critical point of hexadecane and does not end at the critical point of CO<sub>2</sub>. In addition we observe liquid-liquid immiscibility and a three-phase line. When we want to obtain this behavior from our coarse-grained model we must allow for a deviation from the first equation of Eq. (3), assuming rather

$$\varepsilon_{hc} = \xi \sqrt{\varepsilon_{hh} \varepsilon_{cc}}, \quad \xi < 1 \quad . \quad (4)$$

It turns out that a suitable choice for the parameter  $\xi$  which characterizes the deviation from the Lorentz-Berthelot mixing rule is [17, 18, 23]  $\xi = 0.886$ . Eq. (4) with this choice of  $\xi$  was in fact used to compute the phase diagram shown in Fig. 3. However, experimental measurements of the critical line vary considerably and a small modification in  $\xi$  rises or lowers the critical line. Details about how such phase diagrams are in fact estimated from the simulation are given elsewhere [18].

For a study of the phase diagram (Fig. 3) as well as for a study of the interfacial free energy between coexisting gas and liquid phases [17, 18] the grandcanonical ensemble is used, where volume  $V$ , temperature  $T$ , and the

chemical potentials  $\mu_c$ ,  $\mu_h$  are fixed. Both the particle numbers  $N_c$  and  $N_h$  of CO<sub>2</sub> and hexadecane and the pressure  $p$  are then (fluctuating) observables “measured” in the simulation [18]. Fig. 4 shows an isothermal slice through the phase diagram at  $T = 486$  K. This temperature is higher than the temperature of the critical end point where the critical line ending at the critical point of CO<sub>2</sub> and the line of triple points ( $p_{\text{trip}}(T)$ ) in the  $(p, T)$  phase diagram (Fig. 3) meet. Therefore unlike Fig. 2 there is no triple point in the phase diagram, and the qualitative features are the same as in Fig. 1b. At this temperature we shall examine the kinetics of the phase separation in Sec.4.

In order to observe the kinetics of bubble nucleation in the vicinity of the binodal we control the undersaturation of the system by fixing the chemical potential of both species. As a starting configuration we use a homogeneous state equilibrated at a higher temperature. This situation corresponds to a simulation cell in contact with a much larger reservoir which is held at constant undersaturation. As the number of particles in the simulation cell is not conserved, and the particles do not move according to a realistic dynamics, we do not obtain information about the time scale of bubble nucleation. The kinetics of phase separation in the vicinity of the binodal is, however, chiefly determined by the free energy barrier the system encounters on its path towards the equilibrium state. Hence, we expect the relaxation path to be similar to a simulation with realistic dynamics. The most natural choice would be to apply Molecular Dynamics methods [24, 25]. However, if the number of particles was conserved we would need prohibitively large simulation cells for the undersaturation not to decrease substantially even in the very early stages of nucleation. The simulation of spinodal decomposition took place in the canonical ensemble. Again, a homogeneous starting configuration was equilibrated at a higher temperature and quenched to a state below a critical point of the mixture system. We only allowed for local Monte Carlo displacements which should yield kinetics comparable to those obtained in Molecular Dynamics.

### 3 Static equilibrium properties

First we return to the phase diagrams in Figs. 3, 4 and discuss their properties more closely. Note that at the temperature chosen in Fig. 4 ( $T = 486$  K) we are very far below the critical point of pure hexadecane (which is  $T_c = 723$  K). Therefore the hexadecane melt (with some dissolved carbon dioxide) coexists with almost pure CO<sub>2</sub> the composition of which gradually changes from gas- to liquid-like with increasing pressure. In both cases there is almost no hexadecane present. This is reflected in the coexistence curve which rapidly approaches the CO<sub>2</sub> molar fraction  $x = 1$ .

We have also included the results of an analytical approximation for the phase diagram of our model, obtained from a thermodynamic perturbation theory [23] called TPT1, developed along the lines of Wertheim et al. [27]. It is seen that this theory describes the coexistence curve in Fig.4 at pressures that are much smaller than the critical pressure  $p_{\text{crit}}(T)$  almost quantitatively, while the

critical pressure itself is clearly overestimated. Of course, such an overestimation of the critical parameters  $p_{\text{crit}}(T)$ ,  $x_{\text{crit}}(T)$  is quite typical for all theories that invoke a mean field description of the critical behavior, as TPT1 does. A similar analytical study for more alcane-CO<sub>2</sub> systems has been performed recently [28]. Note also that the TPT1 theory readily yields a spinodal curve, which has the standard meaning of separating “metastable states” from “unstable states” in the phase diagram [29, 30, 31]. The naive (mean-field) description implies that in the metastable region of the phase diagram the initial stages of phase separation kinetics are described by nucleation and growth [29, 30], while in the unstable region the decay mechanism is spinodal decomposition [30, 31]. In systems with short range forces there is no well-defined sharp spinodal line, the actual transition between both decay mechanisms occurs rather gradually in a broad transition region, and this region is not centered around the mean field spinodal but occurs close to the coexistence curve [31]. However, for the quenching experiment performed at  $T = 486$  K and  $x = 0.60$ , where the final state corresponds to a pressure of about  $p \approx 130$  bar, we are so close to the coexistence curve and so far from the mean field spinodal, that classical nucleation-type behavior [29, 30] should be observable. In order to demonstrate the mechanism of spinodal decomposition, we quenched into the unstable region as defined by the mean-field spinodal (compare with Fig. 4).

Classical nucleation theory assumes (in our case) the formation of spherical gas bubbles of essentially pure CO<sub>2</sub> within a hexadecane matrix. For a quantitative understanding of the free energy barrier against homogeneous nucleation, clearly the understanding of the interface between macroscopic coexisting phases is a prerequisite. As discussed elsewhere [17, 18], such interfaces are most conveniently studied in the grandcanonical ensemble in conjunction with a multicanonical preweighting scheme that generates mixed-phase configurations. Choosing a simulation box of rectangular shape  $L \times L \times cL$  with a constant  $c = 2$  or larger and periodic boundary conditions, one generates system configurations where the two coexisting phases are separated by two parallel  $L \times L$  interfaces (compare with Fig. 5a). “Measuring” the canonical probability of these two-phase configurations relative to the probability of the pure phases is a standard method for the estimation of interfacial free energies [16, 17, 18, 32, 33, 34, 35, 36, 37]. The results for  $T=486$  K are shown in the inset of Fig. 4. In addition, this method can be used to generate well-equilibrated configurations of interfaces allowing a study of the interfacial structure. Fig. 5 shows, as an example, two snapshot pictures of such states containing interfaces, one at  $T=486$  K and the other at  $T=243$  K. The size of the particles is enlarged (radii shown are  $\sigma_{\text{cc}}$ ,  $\sigma_{\text{hh}}$  rather than  $\sigma_{\text{cc}}/2$ ,  $\sigma_{\text{hh}}/2$ ), for the sake of a clearer view. The temperature  $T=243$  K is slightly lower than the temperature of the critical point of pure CO<sub>2</sub>, and thus the system possesses a triple point where a polymer-rich phase coexists with two CO<sub>2</sub>-rich phases, one being liquid CO<sub>2</sub> and the other the gas. Consequently, when we study the interface between the polymer-rich phase and gaseous CO<sub>2</sub>, a layer of the third phase (liquid CO<sub>2</sub>) intrudes at this interface. The thickness of this layer is expected to diverge when the pressure approaches the value of the triple point pressure.

For higher pressures, we then have a coexistence between the polymer rich-phase and the liquid-like dense  $\text{CO}_2$ , similar to the situation that occurs at the higher temperature (Fig. 5a). At low enough temperatures, where a triple point occurs, one expects a strong decrease of the interfacial tension already when the triple point pressure is approached [11]: the interfacial tension between the polymer-rich phase and liquid-like  $\text{CO}_2$  is much smaller than the interfacial tension between the polymer-rich phase and the gas. The barrier against nucleation also decreases when one approaches the spinodal from the metastable region. This fact facilitates nucleation of relatively large droplets observable on the time-scales of our Monte Carlo simulation.

## 4 Monte Carlo simulation of bubble nucleation

The animation in Fig. 6 visualizes how phase separation in polymer solutions proceeds via nucleation. In the beginning the system fluctuates around a metastable free energy minimum. One observes the “birth and death” of small density fluctuations in the hexadecane matrix (displayed as red spheres) which become visible whenever the blue background shines through the slice. These irregular voids are too small, however, to lead to an immediate decay of the initial metastable state. Usually the voids also contain a few  $\text{CO}_2$  molecules (displayed as small yellow spheres). Only after some time lag a void manages to grow to critical size and overcome the free energy barrier which separates the metastable from the homogeneous equilibrium state. From now on the bubble will grow until it fills the whole simulation box. As expected, the critical void gets also filled with  $\text{CO}_2$  molecules, thus decreasing the supersaturation of the remaining polymer-rich phase. Remarkably, this filling of the bubble does not occur homogeneously: at the interface between the gas and the polymer, i.e., at the surface of the bubble, the  $\text{CO}_2$  density is clearly higher than it is in the center of the bubble. This surface enrichment effect may be interpreted as a precursor to interfacial wetting of the fluid  $\text{CO}_2$  predicted when one approaches the triple point [11]. A quantitative analysis of this phenomena is in preparation [40].

Of course, the observation of a nucleation event displayed in Fig. 6 is by no means the first observation of nucleation phenomena by computer simulations: e.g., already Ref. [29] contains a series of snapshot pictures illustrating nucleation in the two-dimensional lattice gas model. Since then many more elaborate studies have appeared. However, the present work deals with nucleation in a system of industrial relevance, namely bubble nucleation in metastable polymer melts supersaturated with supercritical  $\text{CO}_2$ . In addition, the nucleation mechanism here is quite nontrivial, since the “critical bubble” (which just has the size to be at the nucleation barrier, where there is a 50% chance of growth or decay) is characterized by two variables, its size and the number of  $\text{CO}_2$  molecules it contains. Similarly the interface is described by nontrivial profiles of two variables, the total density and the relative concentration of  $\text{CO}_2$ . Such a nontrivial coupling between two order parameters has also been predicted by

recent self-consistent field calculations based on a qualitatively similar model [11]. Since these mean field descriptions do not take into account the effects of fluctuations, a check by computer simulation methods is clearly warranted.

When we quench to a position below the critical point (Fig. 7), the behavior is rather different: fluctuations in the relative concentration of  $\text{CO}_2$  get gradually more pronounced everywhere. These fluctuations are not localized, however, in the form of identifiable bubbles, but rather form an irregular percolating network. This is the hallmark of spinodal decomposition [30, 31]. Since the linear theory of spinodal decomposition only holds for systems with long range forces in the very early stages [31], we do not attempt a more quantitative analysis of this data. Note also that the build-up of these concentration fluctuations is relatively faster than the nucleation of bubbles. Hence the separation of time scales between the structural relaxation and the rate constant of spinodal decomposition is less well established. In the intermediate stages of spinodal decomposition, we also expect hydrodynamic mechanisms to prevail [30, 31], which are not captured by Monte Carlo moves.

Returning now to the simulation of nucleation phenomena, we ask how one can quantify these observations. A straightforward but tedious method would be to repeat dynamic simulations as shown in Fig. 6 many times in order to extract an estimate of the nucleation rate from the average time it takes to form a bubble or a droplet. Of course, since the nucleation rate is expected to decrease dramatically if the quench depth is decreased slightly, such a direct method works hardly in practice. An indirect method to obtain information on the surface free energy of clusters as a function of cluster size simply uses the final equilibrium states of simulations. An estimate for the free energy as a function of density can be obtained directly from the probability distribution. In this context special care has to be taken of finite-size effects to identify regions of densities which correspond to a single cluster [41, 42]. If we assume that bubbles (or droplets) are spherical, filled with gas and surrounded by a homogeneous liquid of coexistence density (or vice versa), we can assign a radius to each density and hence a free energy estimate to each radius. Fig. 8 indicates that the surface free energy obtained this way is somewhat smaller than expected from the so-called “capillarity approximation”. A simple estimate of the free energy is  $F_s = 4\pi R^2 \gamma_{\text{int}}$ , where  $R$  is the radius of the cluster and  $\gamma_{\text{int}}$  the interfacial tension of flat interfaces as shown in Fig. 5 and derived in Fig. 4. As a consequence, the nucleation barrier is lower than the classical theory of homogeneous nucleation [29, 30] would predict. Differences in  $\gamma_{\text{int}}$  also decrease with increasing cluster size and distance to the critical point of the mixture. At this point, however, the findings are still somewhat preliminary, and more work will be necessary to obtain sufficiently accurate results [43].

## 5 Concluding Remarks

In summary, we have presented a simple model and computational tools which allow us to examine equilibrium properties and kinetics of phase separation



in systems of industrial relevance. We were able to produce a two-component mixture phase diagram with a complete critical line which is in qualitative agreement with experiments. For a system at  $T=486$  K we determined the isotherm and interfacial tension of a flat surface as a function of pressure. In a small animations and a series of snapshots we visualized bubble nucleation and spinodal decomposition for this specific system. For the first case we found a precursor of interfacial wetting which was also observed on a flat surface in the vicinity of the three-phase coexistence line. Finally, we found evidence that for small bubbles the interfacial tension is smaller than expected by classical theory of homogeneous nucleation.

## 6 Acknowledgements

Financial support from the BASF AG (P.V.) and from the Deutsche Forschungsgemeinschaft (DFG) via a Heisenberg fellowship (M.M.) and by grant No BT 314/17-3 (L.G.M) is gratefully acknowledged. LGM would like to thank Ministerio de Ciencia y Tecnologia (MCYT) and Universidad Complutense (UCM) for the award of a Ramon y Cajal fellowship and for financial support under contract BFM-2001-1420-C02-01. We are grateful to E. Hädicke, B. Rathke, R. Strey, and D.W. Heermann for stimulating discussions, and to NIC Jülich, HLR Stuttgart, and ZDV Mainz for generous grants of computer time.

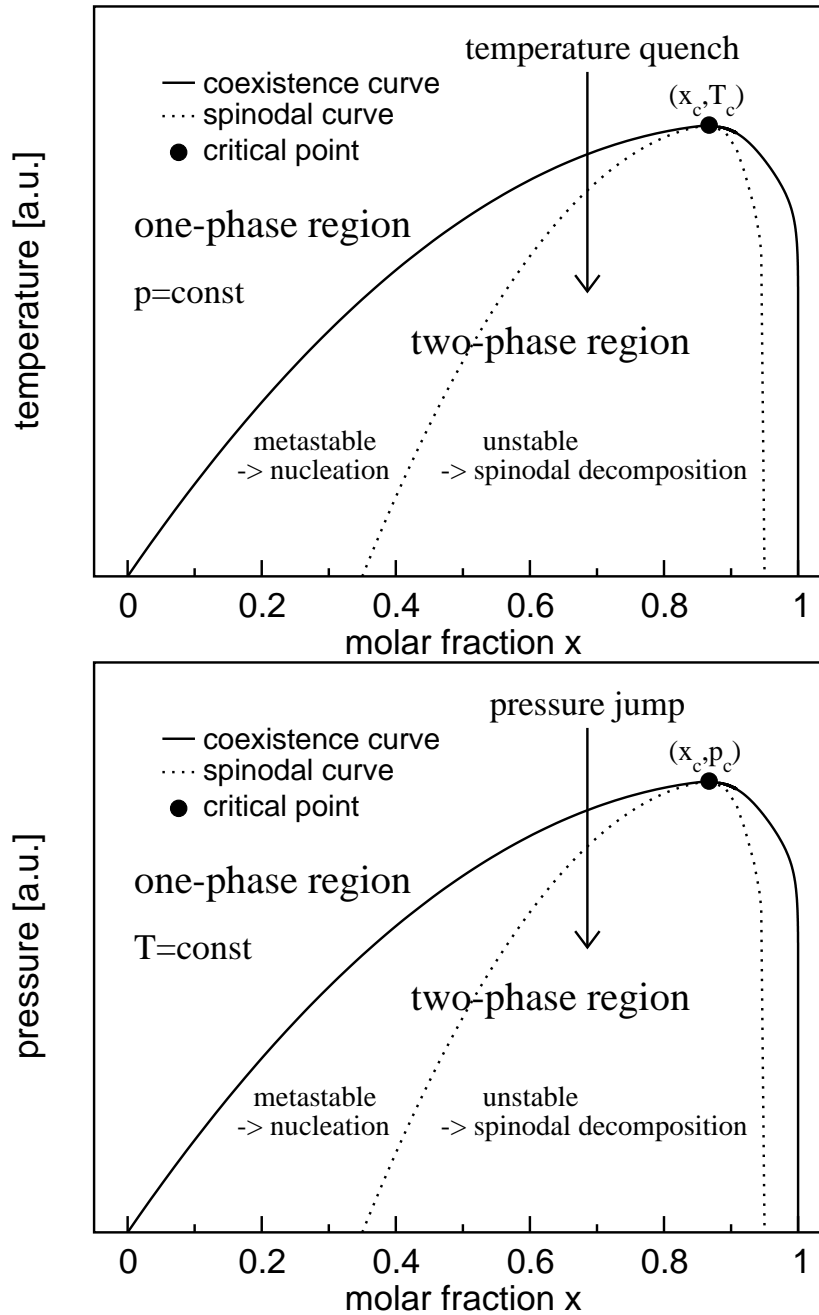


Figure 1: a) Schematic phase diagram of an incompressible polymer solution. Temperature  $T$  and molar fraction  $x$  of the solvent are variables, pressure  $p$  is constant. The position of the critical point is shown by  $\bullet$ . We indicate how a sudden decrease of temperature from a state in the one phase region to a state in the two-phase region is carried out. Note that the molar fraction  $x_c$  of the critical point tends to unity when the chain length  $N$  of the macromolecule gets large. b) Schematic isothermal slice of a phase diagram of a compressible polymer solution, using pressure  $p$  and molar fraction  $x$  of the solvent as variables. We indicate how a pressure jump experiment could be performed. In both cases a) and b) it is assumed that the state after the jump is in the unstable region of the phase diagram, i.e., underneath the spinodal curve. If the quench ends in between the spinodal curve and the coexistence curve, phase separation will start by homogeneous nucleation.

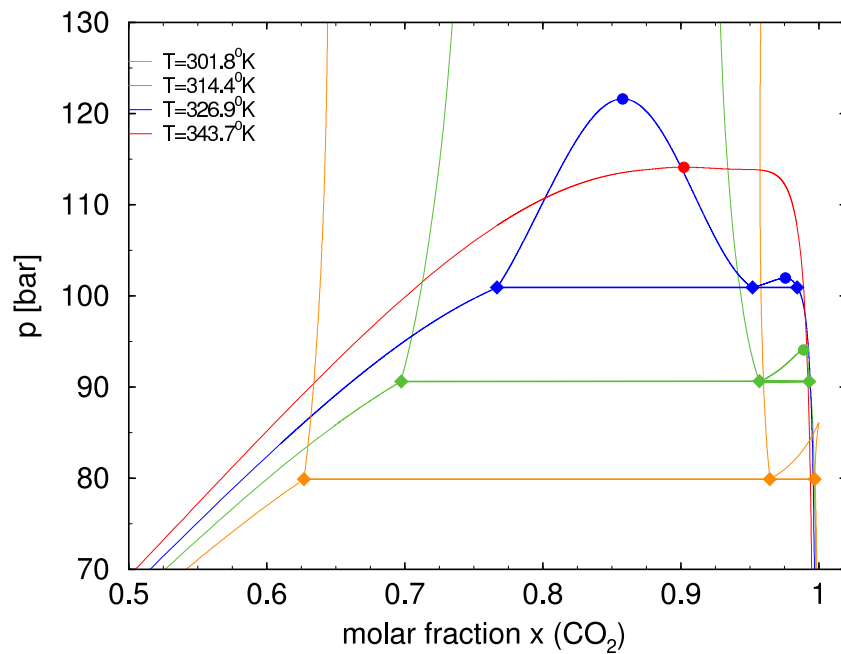


Figure 2: Isotherms of a simple model-system obtained from self-consistent field calculations [11]. At  $T=343.7$  K the phase diagram is like the schematic diagram in Fig. 1b. However, at temperatures close to the critical point of pure  $\text{CO}_2$  we observe liquid-liquid immiscibility for a type III system. A three phase line and a second critical point occur.

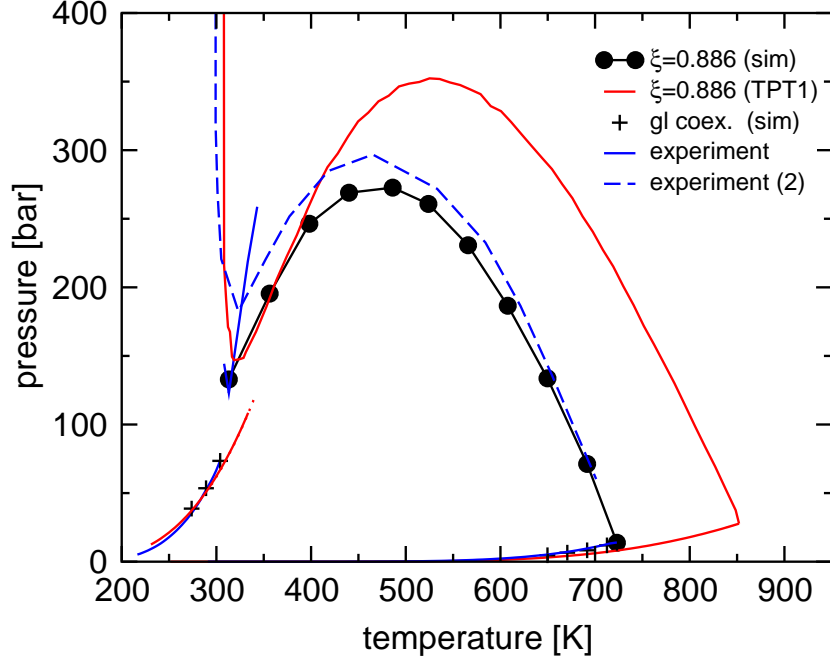


Figure 3: Projection of the hexadecane-CO<sub>2</sub> phase diagram ( $p, T, x$ ) onto the pressure-temperature plane. Black lines, + and  $\bullet$ : simulations (for  $\xi = 0.886$ ), red lines: analytic calculations from a thermodynamic perturbation theory (TPT1) based on the same model [23], blue lines: experimental data. Gas-liquid coexistence lines are from [44, 45], the two critical lines are taken from [39] and [22, 46] (dashed blue) and differ considerably. Experiments are in qualitative agreement with both simulations and analytic calculations. Three features can be identified: Gas-liquid coexistence lines (+) of pure CO<sub>2</sub> and hexadecane both end at the corresponding critical point (at  $T=304$  K and  $T=723$  K respectively). A line of critical points ( $\bullet$ ) emerges from the critical point of pure hexadecane and gradually changes its composition from gas-liquid hexadecane to liquid CO<sub>2</sub> - liquid hexadecane. The red dotted three-phase line (TPT1) lies slightly below the corresponding CO<sub>2</sub> coexistence curve, but only above the critical point of CO<sub>2</sub> it is distinguished in this plot. The critical point of CO<sub>2</sub> and the the end point of the three-phase line are connected by another short critical line which cannot be distinguished, too.

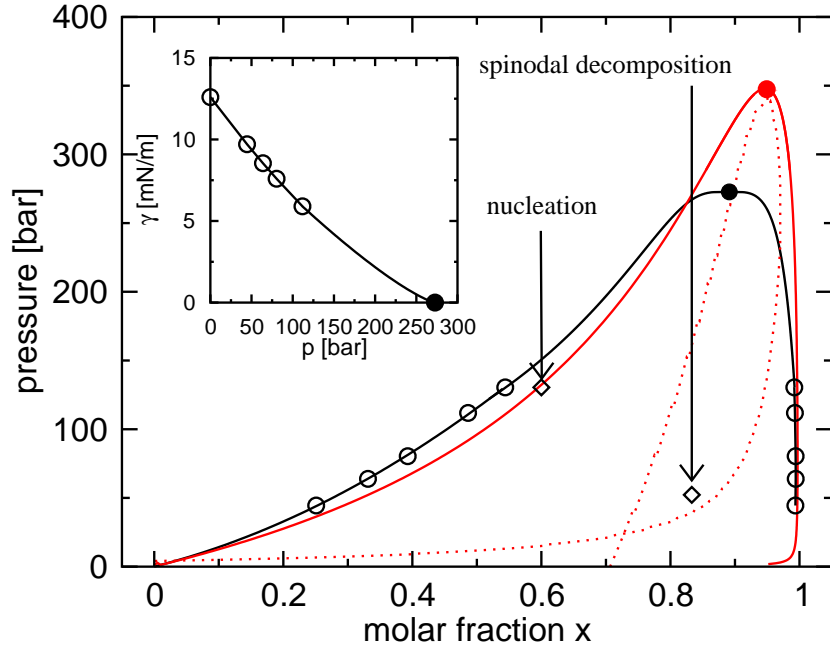


Figure 4: Isothermal slice through the phase diagram in Fig. 3 at temperature  $T=486$  K. Black curve with circles shows the simulated coexistence curve. Red curves are corresponding predictions from TPT1 theory [23] for coexistence (full) and the spinodal curve (dotted), respectively. The position of the critical points are denoted by  $\bullet$ .  $\diamond$  indicate phase diagram positions of nucleation and spinodal decomposition movies in Fig. 6 and Fig. 7. (Inset): surface tension as a function of pressure.

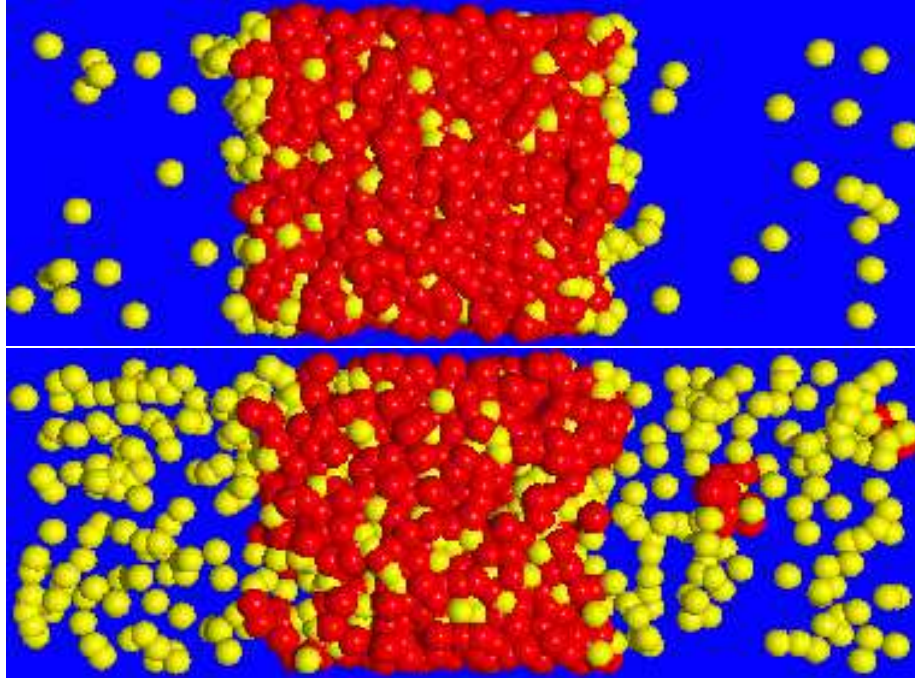


Figure 5: Snapshot pictures of systems in the center of the two-phase coexistence region for  $T=243$  K and  $T=486$  K. Snapshots show a  $2\sigma_{hh}$  slice through a box with dimensions  $L_x \times L_y \times L_z = 18 \sigma_{hh} \times 18 \sigma_{hh} \times 54 \sigma_{hh}$ . Positions of particles are projected into the  $xz$  plane.  $\text{CO}_2$  particles are shown as yellow circles of radius  $\sigma_{cc}$ , while effective monomers of hexadecane are shown as red circles of radius  $\sigma_{hh}$  (we choose  $\sigma_{hh} = 1$  as our unit of length, which then implies  $\sigma_{cc} = 0.816$ ), the background is blue. For  $T=243$  K interfacial wetting can be observed.

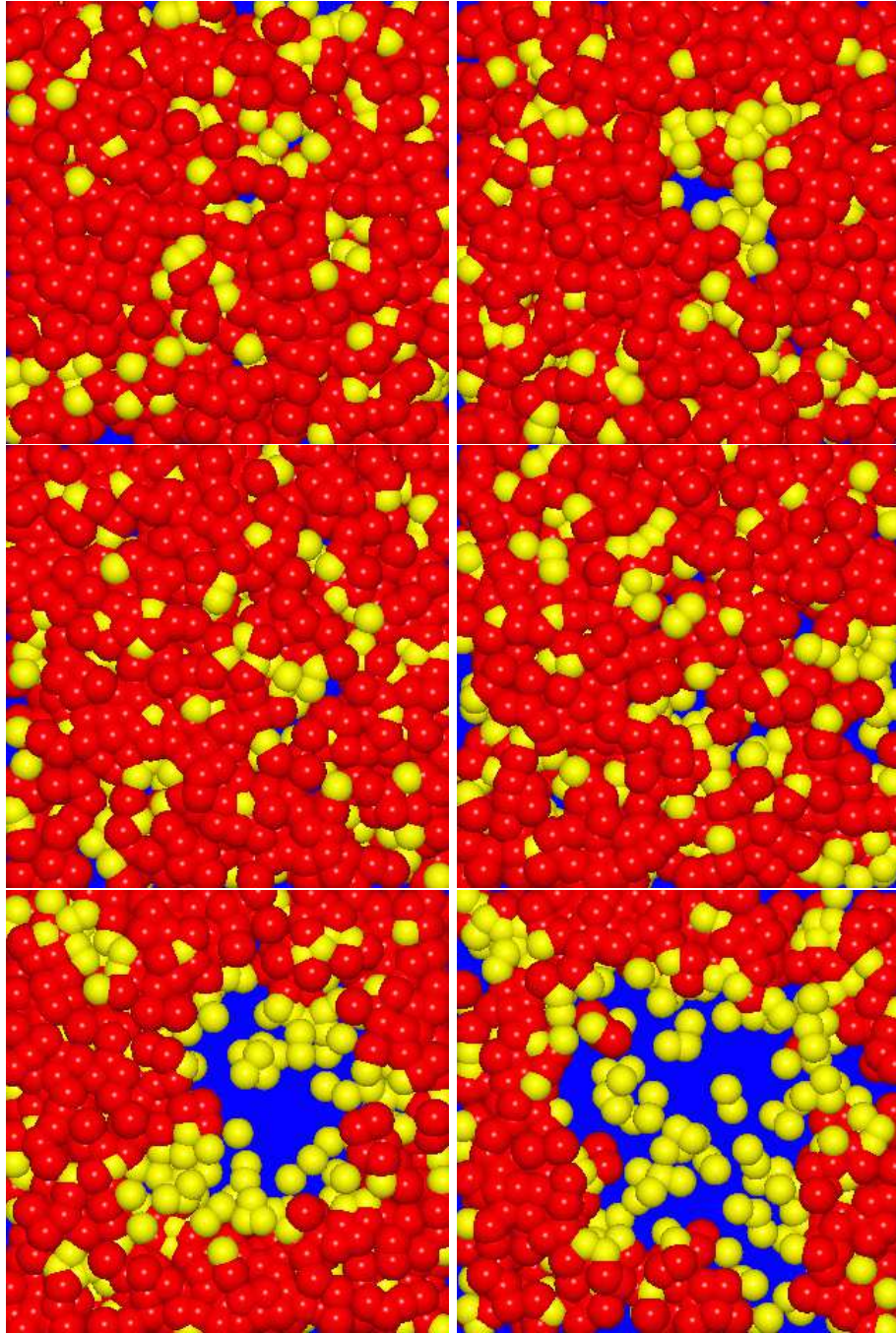


Figure 6: (Remark: The final version (submitted to New Journal of Physics) will contain a short animation. Here, only snap-shot pictures are shown.) A short animation showing the time evolution of a quenching experiment into the metastable region ( $T=486$  K,  $x=0.60$  and (final) pressure  $p \approx 130$  bar - compare with Fig.4). Phase separation occurs via nucleation. The linear dimension of the simulation box is  $22.5 \sigma_{hh}$ . The movie is generated from subsequent snapshot pictures of a grandcanonical Monte Carlo simulation. For clarity, not the whole simulation but only a slice of thickness  $2 \sigma_{hh}$  is shown. The color coding is the same as in Fig. 5.



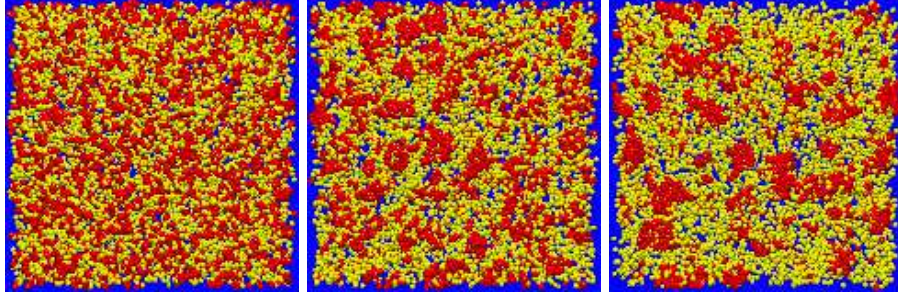


Figure 7: A series of snapshots visualizing the early stages of spinodal decomposition after a quenching experiment into the unstable region ( $T=486$  K,  $x=0.833$  and (final) pressure  $p \approx 52$  bar - compare with Fig. 4). Phase separation occurs via spinodal decomposition. The size of the box is  $91.21 \sigma_{hh} \times 91.21 \sigma_{hh} \times 17.53 \sigma_{hh}$ , but only a slice of  $10 \sigma_{hh}$  is shown. The system is actually more dilute than the one shown in Fig. 6. (a) Starting configuration, (b) after 125000 and (c) after 500000 local displacements ( $0-0.3 \sigma_5$ ) per particle. The color coding is the same as in Fig. 5.



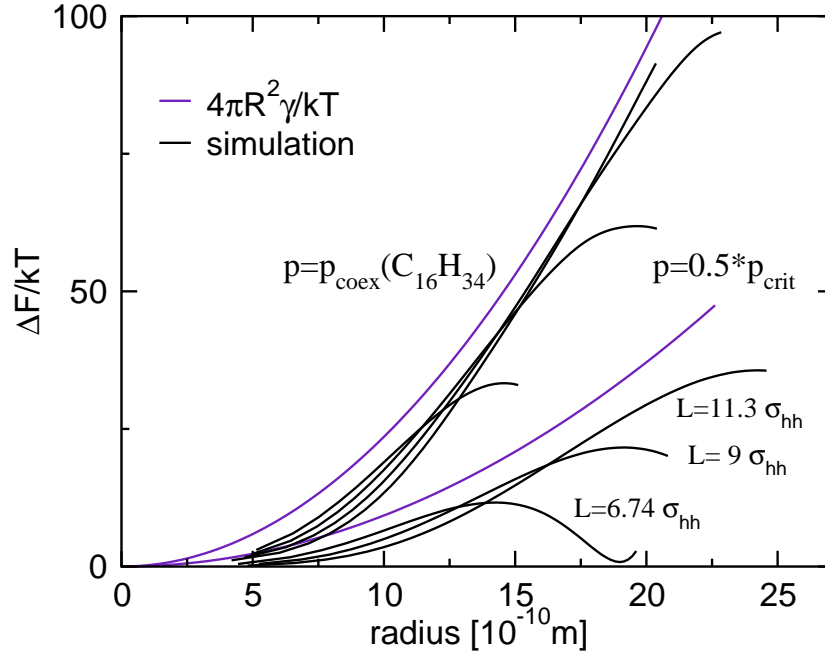


Figure 8: Free energy as a function of droplet size for  $T=486$  K and  $p = 0.5 p_{crit}$  and  $p \approx 0$  (coexistence pressure of pure hexadecane - compare with Fig. 3 and Fig. 4). Indigo line: A simple estimate for the free energy:  $\Delta F = 4\pi\gamma R^2$ , surface tension  $\gamma$  is taken from Fig. 4 (inlet) (flat surface). Black: results from simulations of different system sizes. Only the envelope of the curves is relevant. Other parts of the curves belong to regions of the distribution where no nucleation is expected. For small droplets the free energy is smaller than expected. Differences decrease with increasing radius and decreasing distance from the critical point of the isotherm.

## References

- [1] L. A. Kleintjens, In *Supercritical Fluids*. Kiran, E., Levelt-Sengers, J. M. H., Eds (Kluwer, Dordrecht, 1994)
- [2] Kiran,E., and Brennecke, Eds. *Supercritical Fluid Engineering Science* ACS Symposium Series 514 (American Chem. Soc., Washington D. C., 1993)
- [3] J.H. Han and C.D. Han, J. Polym. Sci., Part B: Polym. Phys. **28**, 711 (1990)
- [4] S.K. Goel and E.J. Beckman, Poly. Eng. Sci. **34**, 1137 (1994); **34**, 1148 (1994)
- [5] C.M. Stafford, T.P. Russell, and T.J. McCarthy, Macromolecules **32**, 7610 (1999)
- [6] B. Krause, H.-J. P. Sijbesma, P. Münüklü, N.F.A. van der Vegt, and W. Wessling, Macromolecules **34**, 8792 (2001); B. Krause, R. Mettinkhof, N.F.A van der Vegt, and M. Wessling, *ibid*, **34**, 874 (2001)
- [7] P.J. Flory, *Principles of Polymer Chemistry* (Cornell University Press, Ithaca, 1953)
- [8] P.J. Flory, J. Chem. **9**, 660 (1941); M.L. Huggins, *ibid*, **9**, 440 (1941)
- [9] K. Binder, J. Chem. Phys. **79**, 6387 (1983); Adv. Polymer Sci. **112**, 181 (1994)
- [10] B. Widom, Physica A**194**, 532 (1993)
- [11] M. Müller, L.G. MacDowell, P. Virnau, and K. Binder, J. Chem. Phys. **117**, 5480 (2002)
- [12] E. Hädicke, H. Schuch, W. Hüttenschmidt, P. Virnau, M. Müller, L.G. MacDowell, K. Binder, B. Rathke, E. Strey, and D.W. Heermann, in preparation.
- [13] W. Paul, G.D. Smith, D.Y. Yoon, B. Farago, S. Rathgeber, A. Zirkel, L. Willner, and D. Richter, Phys. Rev. Lett. **80**, 2346 (1998); W. Paul, AIP Conf. Proc. **469**, 575 (1999)
- [14] K. Kremer and G.S. Grest, J. Chem. Phys. **92**, 5057 (1990)
- [15] C. Bennemann, W. Paul, K. Binder and B. Dünweg, Phys. Rev. E**57**, 843 (1998)
- [16] N.B. Wilding, in *Annual Reviews of Computational Physics* IV. (ed. by D. Stauffer) p.37 (World Scientific, Singapore, 1996); N.B. Wilding, M. Müller, and K. Binder, J. Chem. Phys. **105**, 802 (1996); N.B. Wilding, F. Schmid, and P. Nielaba, Phys. Rev. E**58**, 2201 (1998)

- [17] P. Virnau, M. Müller, L. González MacDowell and K. Binder, *Comp. Phys. Commun.* **147**, 978 (2002)
- [18] P. Virnau, M. Müller, L. González MacDowell, and K. Binder, to be published.
- [19] G.C. Maitland, M. Rigby, E.B. Smith and W.A. Wakeham, *Intermolecular Forces* (Clarendon, Oxford, 1981)
- [20] P. Van Konynenburg and R. L. Scott, *Philos. Trans. R. Soc. London Series A* **298**, 495 (1980)
- [21] J.S. Rowlinson and F.L. Swinton, *Liquids and Liquid Mixtures* (Butterworth, London 1982)
- [22] G.M. Schneider, *Adv. Chem. Phys.* **27**, 1 (1970)
- [23] L.G. MacDowell, P. Virnau, M. Müller, and K. Binder, *J. Chem. Phys.* **117**, 6360 (2002)
- [24] K. Binder and G. Cicotti (eds) *Monte Carlo and Molecular Dynamics of Condensed Matter Systems* (Società Italiana di Fisica, Bologna, 1996)
- [25] K. Binder (ed.) *Monte Carlo and Molecular Dynamics Simulations in Polymer Science* (Oxford, University Press, New York, 1995).
- [26] F. Varnik and K. Binder, *J. Chem. Phys.* **117**, 6336 (2002)
- [27] M.S. Wertheim, *J. Stat. Phys.* **35**, 19, 35 (1984); *ibid*, **42**, 459, 477 (1986); *J. Chem. Phys.* **85**, 2929 (1986); *ibid*, **87**, 7323 (1987); W.G. Chapman, G. Jackson, and K.E. Gubbins, *Mol. Phys.* **65**, 1057 (1988)
- [28] A. Galindo and F. J. Blas, *JPC-B*, **106**, 4503 (2002)
- [29] K. Binder and D. Stauffer, *Adv. Phys.* **25**, 343 (1976)
- [30] J.D. Gunton, M. San Miguel, and P.S. Sahni, in *Phase Transitions and Critical Phenomena, Vol 8* (edited by C. Domb and J.L. Lebowitz), p. 267 (Academic Press, London, 1983)
- [31] K. Binder and P. Fratzl, in *Phase Transformations of Materials* (ed. by G. Kostorz) p. 409 (Wiley-VCH, Weinheim, 2001)
- [32] K. Binder, *Phys. Rev. A* **25**, 1699 (1982)
- [33] B.A. Berg, V. Hansmann, and T. Neuhaus, *Phys. Rev. B* **47**, 497 (1993); *Z. Phys. B* **90**, 229 (1993)
- [34] M. Müller, K. Binder, and W. Oed, *J. Chem. Soc., Faraday Trans.* **91**, 2369 (1995)
- [35] J.E. Hunter, III, and W.P. Reinhardt, *J. Chem. Phys.* **103**, 8627 (1995)

- [36] J.J Potoff and A.Z. Panagiotopoulos, J. Chem. Phys. **112**, 6411 (2000)
- [37] T.S. Jain and J.J. de Pablo, preprint
- [38] K. Binder and M.H. Kalos, J. Stat, Phys. **22**, 363 (1980); K. Binder, Physica A, in press (2002)
- [39] T.Charoensombut-Amon, R.J. Martin, and R.Kobayashi, Fluid Phase Equilibria. **38**, 89 (1986)
- [40] Y. Lin, M. Müller, and K. Binder, to be published.
- [41] L. González MacDowell, P. Virnau, M. Müller, and K. Binder, to be published
- [42] P. Virnau, L. González MacDowell, M. Müller, and K. Binder, cond-mat/0303642
- [43] P. Virnau, M. Müller, L. González MacDowell, and K. Binder, to be published
- [44] R. Span and W. Wagner, JPCRD **25**, 1509 (1996)
- [45] B. D. Smith and R. Srivastava, Elsevier, Amsterdam (1986)
- [46] G. Schneider, Z. Alwani, W. Heim, E. Horvath, and E.U. Franck, Chem. Ingr. Tech., **39**, 649 (1967)